Bulletin of the Seismological Society of America, Vol. 100, No. 3, pp. 1153–1164, June 2010, doi: 10.1785/0120090180

The Long-Lasting Aftershock Series of the 3 May 1887 M_w 7.5 Sonora Earthquake in the Mexican Basin and Range Province

by Raúl R. Castro, Peter M. Shearer, Luciana Astiz, Max Suter,* Cesar Jacques-Ayala, and Frank Vernon

Abstract We study local and regional body-wave arrival times from several seismic networks to better define the active regional fault pattern in the epicentral region of the 3 May 1887 M_w 7.5 Sonora, Mexico (southern Basin and Range Province) earthquake. We determine hypocenter coordinates of earthquakes that originated between 2003 and 2007 from arrival times recorded by the local network RESNES (Red Sísmica del Noreste de Sonora) and stations of the Network of Autonomously Recording Seismographs (NARS)–Baja array. For events between April and December 2007, we also incorporated arrival times from USArray stations located within 150 km of the United States–Mexico border. We first obtained preliminary earthquake locations with the Hypoinverse program (Klein, 2002) and then relocated these initial hypocenter coordinates with the source-specific station term (SSST) method (Lin and Shearer, 2005). Most relocated epicenters cluster in the upper crust near the faults that ruptured during the 1887 earthquake and can be interpreted to be part of its long-lasting series of aftershocks. The region of aftershock activity extends, along the same fault zone, 40–50 km south of the documented southern tip of the 1887 rupture and includes faults in the epicentral region of the 17 May 1913 (I_{max} VIII, M_I 5.0–0.4) and 18 December 1923 (I_{max} IX, M_I 5.7–0.4) Granados–Huásabas, Sonora, earthquakes, which themselves are likely to be aftershocks of the 1887 event. The long aftershock duration can be explained by the unusually large magnitude of the mainshock and by the low slip rates and long mainshock recurrence times of the faults that ruptured in 1887.

Introduction

North–south striking, west-dipping Basin and Range Province normal faults and associated half-grabens form the western edge of the Sierra Madre Occidental plateau in northeastern Sonora, Mexico (Fig. 1). Slip in 1887 within this segmented normal-fault array caused the largest historical earthquake of the southern Basin and Range tectonic-physiographic province and produced the world's longest recorded normal-fault surface rupture in historic time (dePolo *et al.*, 1991; Yeats *et al.*, 1997). Field observations indicate that three major range-bounding normal faults ruptured sequentially in the 1887 Sonora earthquake (Suter and Contreras, 2002; Suter, 2008a, 2008b). The surface rupture dips ~70° W, has an end-to-end length of 101.8 km and a maximum structural displacement (net slip) of 5.2 m, and is composed (from north to south) of the Pitáycachi, Teras, and Otates segments (Fig. 1). Scaling relations between surface rupture length and moment magnitude for normal faults (Wells and Coppersmith, 1994) indicate an M_w of 7.5 ± 0.3 for this earthquake. The rupture is characterized by east–west extension, perpendicular to the fault trace. The regional cross sectional extension by subvertical Basin and Range Province faults is 10% (Suter, 2008a) and was initiated ~23 m.y.a., as indicated by the age of basalt flows intercalated with the lowermost fill of nearby extensional basins.

Long-term slip rates are 0.015 mm/yr for the Pitáycachi (Bull and Pearthree, 1988), 0.08 mm/yr for the Teras, and 0.06 mm/yr for the Otates fault (Suter, 2008a, 2008b). From these slip rates, it can be inferred that, compared to Teras and Otates, Pitáycachi is a more strongly locked fault, with a higher effective coefficient of friction, and experiences higher stress drops. The recurrence intervals of 1887-sized events are 100–200 k.y. for the Pitáycachi fault (Bull and Pearthree, 1988) but only 15–26 k.y. for the Teras fault (Suter, 2008b) and 30–42 k.y. for the Otates fault (Suter, 2008a), which indicates that the Pitáycachi fault only infrequently ruptures together with the Teras and Otates faults. These estimates are within the range of recurrence intervals

*Now at Swiss Federal Nuclear Safety Inspectorate ENSI, CH-5200 Brugg, Switzerland.

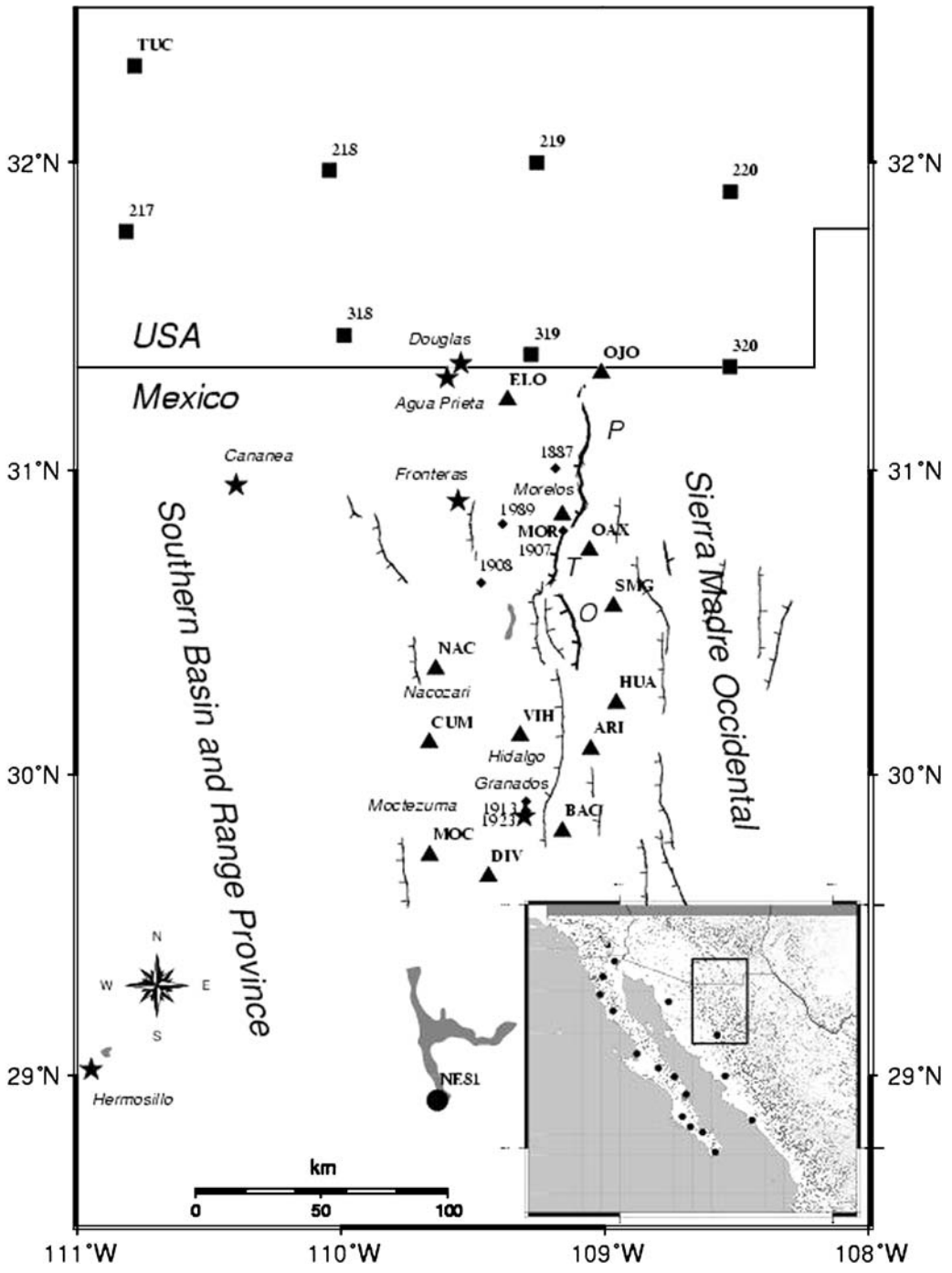

Figure 1. Location of the area studied. Triangles are stations of the RESNES seismic network; squares are USArray stations; circle is a NARS station; and stars indicate major towns. Also shown are the traces of major Basin and Range Province faults (barb symbols on hanging wall, modified after Suter and Contreras, 2002). The faults that ruptured in 1887 (from north to south: P, Pitáycachi; T, Teras; and O, Otates) are highlighted by bold traces. The inset provides a regional view of northwestern Mexico and shows the stations of the NARS–Baja array. The major historical earthquakes are marked by a diamond and the year of their occurrence (from Suter, 2001, table 1).

documented for normal faults of the southern Basin and Range Province and the Rio Grande rift (10–100 k.y.; Pearthree and Calvo, 1987; Menges and Pearthree, 1989; Machette, 1998). The surface rupture along the Pitáycachi segment has a well-developed bilateral branching pattern. This suggests that the rupture of the Pitáycachi segment initiated in its central part where the polarity of the rupture bifurcations changes. It is therefore likely that the rupture first propagated bilaterally along the Pitáycachi fault, from where the southern rupture front cascaded across stepovers first to the Teras fault and then to the Otates fault. Correspondingly, the intensity distribution of this earthquake (Aguilera,

1888; Sbar and DuBois, 1984) indicates a strong rupture directivity effect toward the south.

In this article, we study local and regional body-wave arrival times from several seismic networks to better define the active regional fault pattern in the epicentral region of the 1887 earthquake. In 2002, the Centro de Investigación Científica y de Educación Superior de Ensenada (CICESE), in collaboration with the Instituto de Geología, Universidad Nacional Autónoma de México (UNAM), installed RESNES (Red Sísmica del Noreste de Sonora), a seismic network surrounding the surface rupture of the 1887 earthquake (Castro *et al.*, 2002, 2008). Furthermore, the Network of Autonomously Recording Seismographs (NARS)-Baja, a broadband array surrounding the Gulf of California (Trampert *et al.*, 2003; Clayton *et al.*, 2004), has several stations directly southwest of the 1887 surface rupture. In addition, several USArray stations are located north of the 1887 surface rupture. Figure 1 shows stations of these networks located near the 1887 rupture, and Table 1 provides their coordinates.

At a plate boundary, aftershock sequences are relatively short (< 10 yr). Steady plate motion quickly reloads the fault and thus overwhelms the postseismic stress heterogeneities that cause aftershocks (Stein and Liu, 2009). In contrast, in the Basin and Range Province, faults are reloaded much more slowly, allowing aftershocks to continue much longer.

Table 1
Station Coordinates

Network	Code	Latitude North	Longitude	Altitude
RESNES	MOC	29.73233	−109.66533	621.0
	MOR	30.85117	−109.16267	998.0
	BAC	29.81117	−109.16300	778.0
	VIH	30.12717	−109.32317	610.0
	SMG	30.55317	−108.96983	945.0
	OAX	30.73650	−109.06050	902.0
	NAC	30.34567	−109.64333	1261.0
	ELO	31.22750	−109.37083	1210.0
	OJO	31.31500	−109.01555	1454.0
	DIV	29.66183	−109.44333	745.0
	CUM	30.10450	−109.66700	1243.0
	HUA	30.23433	−108.95867	1181.0
	ARI	30.08217	−109.05500	1546.0
NARS	NE80	30.50000	−112.31983	225.0
	NE81	28.91833	−109.63633	295.0
	NE82	26.91567	−109.23083	183.0
	NE75	27.22933	−112.85650	137.0
	NE76	26.88900	−111.99900	35.0
	NE77	26.01583	−111.36133	40.0
USArray	TUC	32.30980	−110.78470	910.0
	116A	32.56180	−111.70420	477.3
	216A	32.00220	−111.45740	908.0
	217A	31.77480	−110.81620	1412.0
	218A	31.97370	−110.04640	1486.0
	319A	31.37570	−109.28090	1187.0
	318A	31.43900	−109.99070	1576.0
	219A	31.99890	−109.25920	1581.0
	119A	32.76630	−109.30290	1406.0
	117A	32.57160	−110.73930	1544.0
	214A	31.95590	−112.81150	543.0

The earliest historical earthquakes in the Basin and Range Province and the continental interior, which occurred in the eighteenth century, still produce aftershocks. In our analysis we consider aftershocks to be earthquakes that occur after a large event in regions where the deformation is close to zero and the motions of the fault segments that ruptured during the main event are very small. Thus, postmainshock seismicity in regions where there is no evidence of ongoing strain accumulation will be considered aftershocks.

Previous Studies

A map and a parametric catalog of the historical seismicity in the epicentral region of the 1887 Sonora earthquake were presented by Suter (2001). The 1887 rupture has a long history of observed aftershocks. The contemporary field studies by Goodfellow (1888) and Aguilera (1888) (for a summary see Suter, 2006) located aftershocks in the stepover between the Pitáycachi and Teras rupture segments (Fig. 1) based on felt reports and observations with an improvised seismoscope. Contemporary aftershocks were also reported from the region of the Otates rupture segment (Vázquez, 1887). Three compilations of aftershocks in 1887 can be found in the seismicity catalogs by Orozco y Berra (1887, 1888). Aguilera (1888, p. 36) noted that the aftershock activity decayed with time.

A major aftershock occurred on 26 May 1907 (I_{max} VIII, M_I 5.2–0.4). Gridding the intensity values with a Kriging algorithm (Suter, 2001) placed the area of maximum intensity near the stepover between the Pitáycachi and Teras rupture segments of the 1887 earthquake. The 1907 earthquake (Fig. 1) is likely to have been caused by an increase of static Coulomb stress at the tips of these two rupture segments (Suter and Contreras, 2002).

The aftershock activity then migrated south along the same fault system. A major earthquake on 17 May 1913 (I_{max} VIII, M_I 5.0–0.4) destroyed a third of the buildings in Huásabas and caused major damage to the town hall, schoolhouse, and prison (Suter, 2001). In 1923, a shock on 18 December, 5 a.m. local time, destroyed most adobe constructions in Huásabas and Granados (Fig. 1). A second major shock (I_{max} IX, M_I 5.7–0.4) on 19 December, 6 a.m. local time, razed the two villages and was followed by 27 aftershocks on the same day. This earthquake was followed by a series of aftershocks that lasted at least until April 1924 (for details and sources, see Suter, 2001). Stress loading by the 1887 rupture on the fault segments near Granados may explain these two earthquakes (Suter and Contreras, 2002).

Between 1978 and 1979, a temporal network of 7–10 portable seismographs, installed by Natali and Sbar (1982) in the region of the Pitáycachi fault, recorded about 30 small events ($M < 2$), about one event per day of recording. The well-located microearthquakes had horizontal location errors < 5 km and originated at < 15 km depth to the west of the Pitáycachi fault trace, near the northern and southern terminations of the Pitáycachi segment of the 1887 surface

rupture. Composite focal mechanisms by Natali and Sbar (1982) for well-located microearthquakes suggest normal dip slip with a minor right-lateral strike-slip component near the northern tip and normal dip slip near the southern tip of the Pitáycachi rupture segment. Some events were also located farther south, beyond the network, near what is known now as the Teras and Otates segments of the 1887 surface rupture (Fig. 1).

A series of earthquakes in this region in 1987–1989 was relocated by Wallace *et al.* (1988) and Wallace and Pearthree (1989) about 20 km west of the traces of the Teras fault and the southernmost part of the Pitáycachi fault. For the largest of these events, which originated on 25 May 1989 (Fig. 1), Wallace and Pearthree (1989) give a magnitude of 4.2 and estimate the accuracy of its location as ±4 km in the east–west direction and ±5 km in the north–south direction. Three of the microearthquakes recorded by Natali and Sbar (1982) and the epicenter of the 7 April 1908 M_I 4.8 Fronteras earthquake (Suter, 2001) also fall close to this cluster. Coulomb stress modeling (Suter and Contreras, 2002, fig. 3) suggests that this seismicity cluster is located in a region where the 1887 earthquake caused an increase in static shear stress. The focal mechanism for the 25 May 1989 event determined by Wallace and Pearthree (1989) indicates dip slip with a minor left-lateral strike-slip component on the 65° W dipping nodal plane (Suter and Contreras, 2002, fig. 2). This focal mechanism is practically identical with the focal mechanism presentation of the striations measured on the Teras fault surface (Suter, 2008b), which suggests that this earthquake may have had its source on the Teras fault.

More recently, a series of earthquakes with magnitudes $M_L \leq 4.0$ took place in the Granados–Huásabas region in 1993 (Suter, 2001, table 1).

Data

We picked arrival times of *P* and *S* waves recorded by the stations of the RESNES array (Fig. 1, Table 1) during the period 2003–2007. The stations of this deployment consist of Kinemetrics digital recorders (model K2) with internal Epi-Sensors that record the three components of ground acceleration. An additional channel records the vertical component of ground velocity with an external short period seismometer (model L4C). All the stations are autonomous and have a built-in Global Positioning System for time reference. Figure 2 shows a sample of six velocity records from an *M* 2.8 earthquake located on the Pitáycachi fault (30.889° N, 109.236° W) at a depth of 10 km. To better define the regional seismicity, we also picked arrival times from three stations of the NARS-Baja array (Trampert *et al.*, 2003; Clayton *et al.*, 2004) installed in the State of Sonora, NE80, NE81, and NE82. For events that originated south of the RESNES array, we also used arrival times from the NARS-Baja stations NE75, NE76, and NE77, located in Baja California Sur. The coordinates of these six stations are listed in Table 1. We used a computer routine to search for events recorded by three or more stations to manually pick the *P* and *S* wave arrivals and to locate the epicenters.

For relocation purposes, we also used arrival times recorded in 2007 from USArray stations located within about 150 km of the United States–Mexico border. The initial

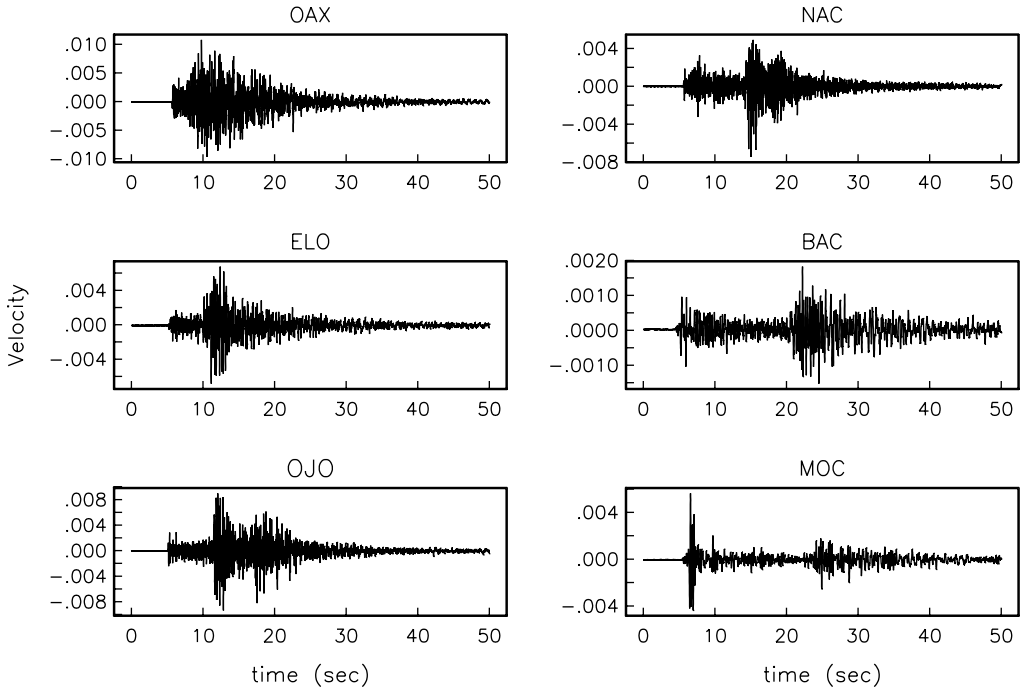

Figure 2. Vertical velocity records from an earthquake (*M* 2.8) that occurred on 6 June 2004 at 10:47 UTC on the Pitáycachi fault (30.889° N, 109.236° W) at a focal depth of 10 km.

data set consists of nearly 600 local and regional events ($M < 3.6$) recorded at a minimum of three stations and permitting at least five reliable phase picks. We estimated the magnitudes of the events using the average duration of the records. We were able to relocate 80% of the events.

Methodology

We determined initial hypocentral locations with the Hypoinverse computer code (Klein, 2002) using arrival times from stations of the RESNES and NARS-Baja arrays. We used the four-layer velocity model (Table 2 and model V1 in Fig. 3) by Harder and Keller (2000), which was determined from a wide-angle seismic profile in adjacent southwestern New Mexico. The model assumes the crust to consist of flat layers of uniform thickness. The uppermost layer is 1-km thick and accounts for sedimentary and volcanic rocks. The second layer corresponds to the crystalline upper crust with a thickness of 21 km. The third layer represents the lower crust, with a thickness of 13 km, and is delimited at its base by the Moho. Table 2 lists the *P*-wave velocities of this model; to calculate *S*-wave velocities, we used a V_P/V_S ratio of 1.75.

Standard methods to locate earthquakes, like Hypoinverse, use static station terms (ST) to account for lateral heterogeneities of the velocity structure. The ST correction is determined by the mean of the travel-time residuals from all the events recorded at a given station. This approach is adequate if the source-station paths are the same for all the events; for example, in the case of localized earthquake clusters. However, in cases where the seismicity is distributed over a large region or consists of several clusters of events, location methods based on static station terms do not account for the travel-time perturbation introduced by lateral velocity heterogeneities. For such cases, Richards-Dinger and Shearer (2000) proposed the use of source-specific station terms (SSST). With this technique, each station has a station correction function that varies with source position. This location method is useful when the seismic events cover a large region with lateral velocity heterogeneities, as can be expected for northeastern Sonora.

A generalization of the SSST method was recently implemented by Lin and Shearer (2005) in their COMPLOC earthquake location code. This new technique consists of selecting nearby events that are located within a sphere of specified radius (r_{max}) around the target event. The SSST of the target event is then determined iteratively by the mean of travel-time residuals from the nearby events, shrinking the cutoff distance r_{max} between the first and the final iterations.

Table 2

P-Wave Velocity Model Used for Initial Hypocentral Locations

Depth Intervals (km)	V_P (km/sec)
0.0–1.0	5.10
1.0–22.0	5.88
22.0–35.0	6.90
Below 35.0	7.95

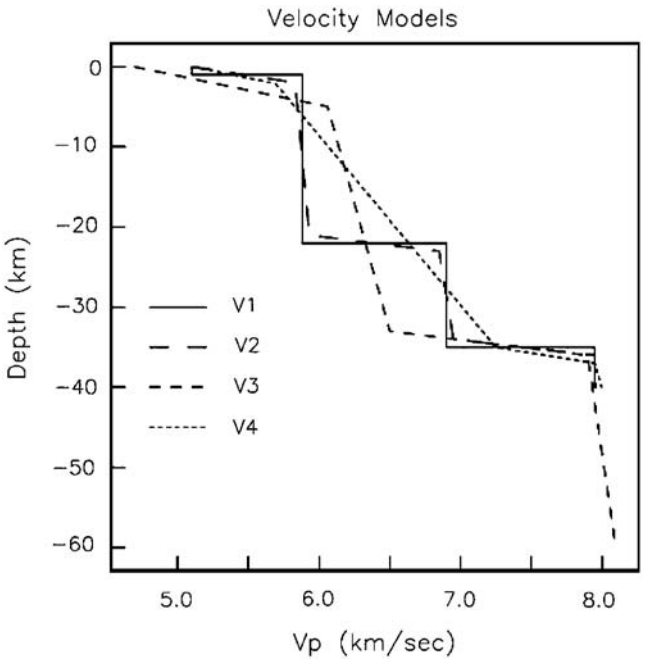

Figure 3. *P*-wave velocity models tested in the relocation of the seismic events. Model V1 was obtained by Harder and Keller (2000) for southwestern New Mexico; model V2 is similar to V1 but contains velocity gradients rather than sharp discontinuities; model V3 is similar to the model used by Lin *et al.* (2007) to locate southern California seismicity; and V4 is the final model used to relocate the hypocenters.

We relocated the initial hypocenters with a modified version of the COMPLOC code that permits the use of regional phases (*Pn*, *Pg*, *Sn*, *Sg*) and weights the phase arrival picks according to the source-station distance. In addition to the arrival times from the local stations of the RESNES array and the regional stations of the NARS-Baja array, we also incorporated body-wave arrivals recorded for the year 2007 by broadband stations of the USArray installed within 150 km of the United States–Mexico border. We start with a velocity model similar to that proposed by Harder and Keller (2000) but introduce small gradients (model V2 in Fig. 3) to make the change of velocity with depth gradual, as is expected in nature. To minimize regional variations of the velocity structure, we relocate the events by dividing the study area into five rectangles, based on the distribution of the epicenters located with Hypoinverse (Fig. 4). One of the rectangles covers the area near Cananea, northwest of the RESNES array; three rectangles cover the fault segments that ruptured in 1887; and the last rectangle, southeast of the network, covers the events located near the Mulatos, Sonora, gold mine in the Sierra Madre Occidental. These rectangles are outlined in Figure 4. We relocated the earthquakes from each of these groups separately. To find the hypocenter coordinates, we used the least absolute value (L1 norm) as the misfit norm because it weights residuals more equally in the inversion.

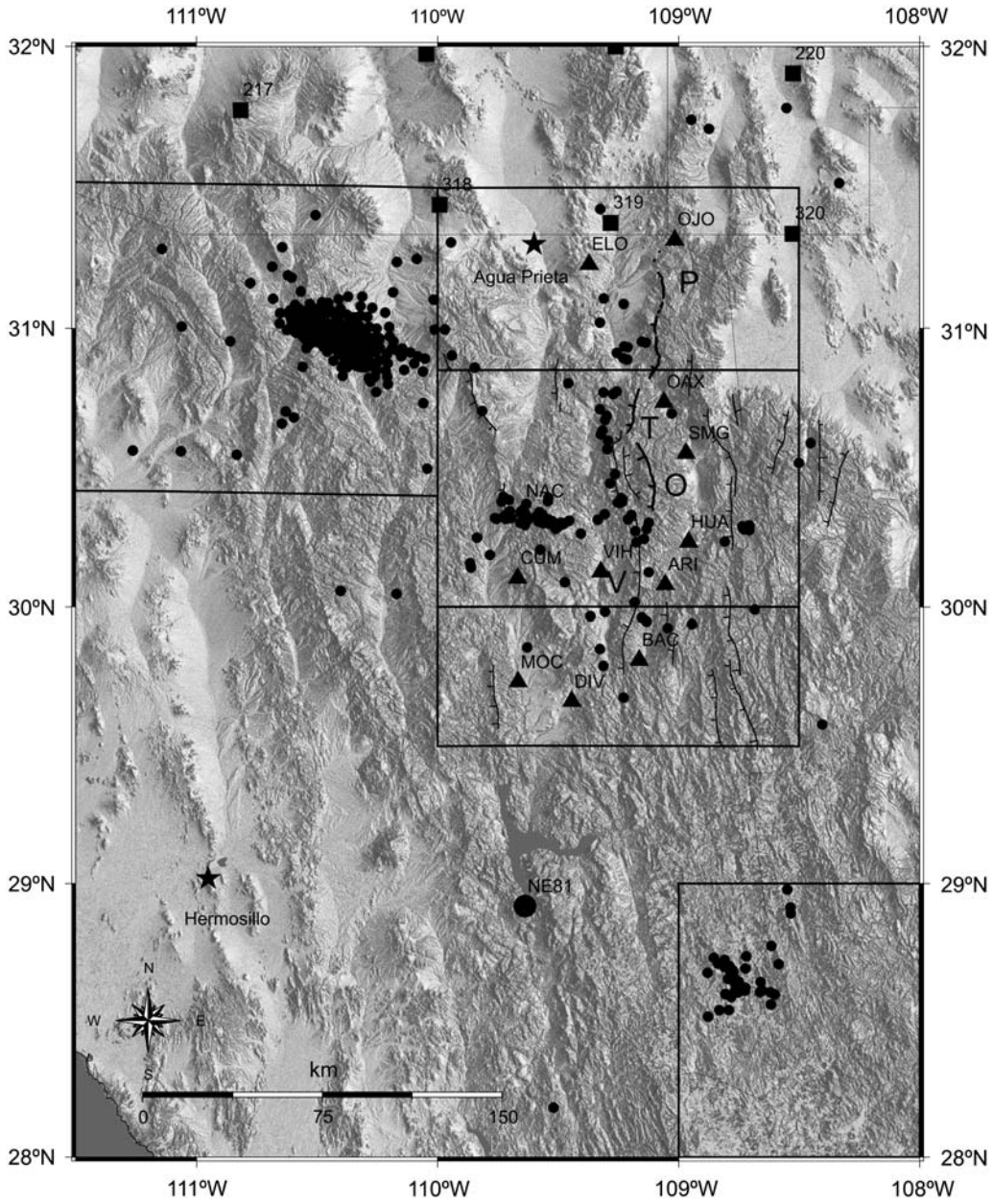

Figure 4. Distribution of hypocenters located with the Hypoinverse code. The faults that ruptured in 1887 (P, Pitáycachi; T, Teras, and O, Otates) are highlighted by bold traces. The solid circle is station NE81 of the NARS–Baja array; solid triangles show the location of RESNES stations; squares show the location of USArray stations used; solid black circles are the epicenters; and V represents the Villa Hidalgo fault. The boundaries of the five rectangles are used to subdivide the seismicity for relocation purposes.

This norm is also robust when outliers are present in the data. Shearer (1997) and Astiz *et al*. (2000) show that in California the epicentral locations have less scatter when the L1 norm is used instead of the conventional least squares method (L2 norm). We tested various velocity models and compared the travel-time residuals to select the model that, on the average, gives the smallest residuals and consequently the best solution. Besides models V1 and V2 (described previously), we tested model V3 (Fig. 3), which is similar to the *P*-wave velocity model used by Lin *et al*. (2007) to locate southern California seismicity. The velocity model V4 is our final selection that we used to relocate the hypocenters.

Results

The epicenters located with Hypoinverse are displayed in Figure 4. Three groups of events can be recognized. The first group, evaluated in more detail below, corresponds to earthquakes distributed along the Basin and Range Province faults on the western margin of the Sierra Madre Occidental, including the faults that ruptured in 1887. The second group clusters near Cananea in the northwest, where a major copper mine is located. In this region, there are also three other mines: María mine, located off the Cananea-Imuris highway, Mariquita mine located further northwest, and the Milpillas

mine. Although we tried to eliminate quarry blasts from the data set based on the correlation of the origin time with the time window of the scheduled mine explosions, it is very likely that most of the events in this group are man-made, particularly the events with a shallow focus of less than 2 km. However, natural seismicity does also occur in this region. For example, on 16 October 1999, the PDE (Preliminary Determinations of Epicenters) catalog located a M_L 4.5 earthquake, which was triggered by the M_w 7.1 Hector Mine earthquake, somewhat southeast of this cluster. The third group of events is located farther southwest, beyond the RESNES and NARS-Baja arrays, near the Mulatos gold mine. These events are likely to be quarry blasts.

In Figure 5, we compare the depth distributions of the original focal locations obtained with Hypoinverse (top row) and the relocated hypocenters obtained with the SSST method (middle and bottom rows) using velocity model V4 (Fig. 3). In the left column, the foci are projected into an east–west section and in the central column into a north–south section. The focal depths of the relocated events are more reliable than those of the original locations. The relocated events are better constrained because we used more arrival times; in addition to time picks from the local RESNES network, we also used regional arrivals from the broadband stations of the USArray and the NARS-Baja array. In the depth distribution of the relocated earthquakes (middle row in Fig. 5), most hypocenters (85%) are above 25 km depth and the majority (69%) above 15 km, which suggests that most of the seismic activity takes place in the upper crust. This is in agreement with observations elsewhere that continental

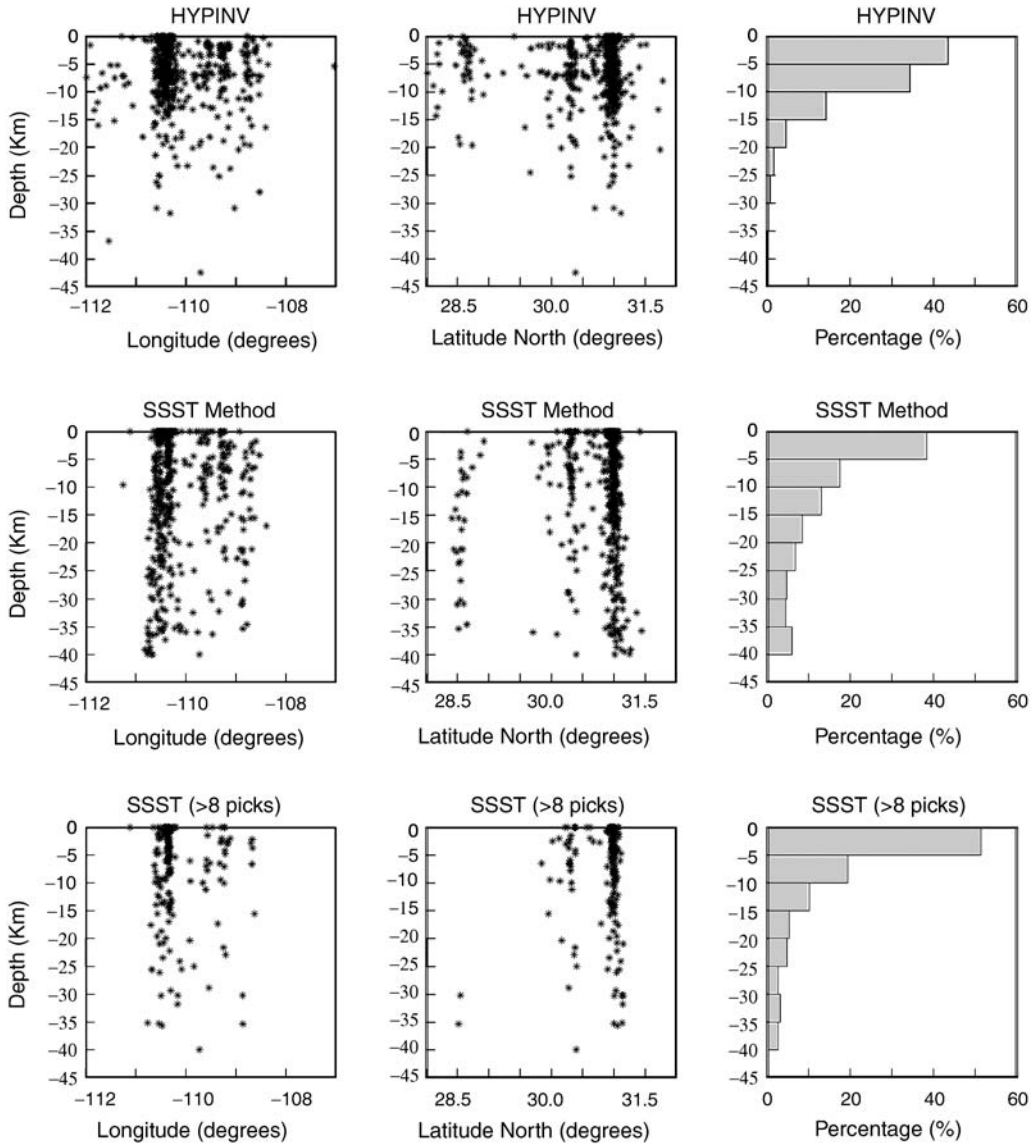

Figure 5. Focal depths obtained with Hypoinverse and velocity model V1 (top row) and with the SSST method and velocity model V4 (middle and bottom rows). In the left column, the foci are projected into an east–west section and in the central column into a north–south section. The right column shows the corresponding histograms. The frames at the bottom show the best constrained events; they were relocated using more than eight arrival picks.

seismicity is confined to the upper half of the crust (Jackson, 2002). The bottom frames in Figure 5 show the best constrained events, namely the ones relocated with more than eight arrival picks; 81% of these events have focal depths of less than 15 km and 71% of less than 10 km. This is in agreement with the depths of the well-located microearthquakes in the vicinity of the Pitáycachi fault in the study by Natali and Sbar (1982) and elsewhere in the Basin and Range Province, where the focal depth of most earthquakes is less than 15 km (Parsons, 1995).

To compare the residuals of the hypocenters located with Hypoinverse with those located with the SSST method, we plotted a histogram (Fig. 6) of the average absolute values of the travel-time residuals. In the histogram, the residuals that resulted from using Hypoinverse (solid lines) are compared with the residuals that resulted from using the modified version of the COMPLOC program with the V2 velocity model (dashed lines) and the V4 velocity model (dotted lines). In the bin for the smallest residuals (Fig. 6), the percentage of events located with the SSST method is higher than the percentage located with Hypoinverse, and the highest percentage (best solution) corresponds to the events where the velocity model V4 (Fig. 3) was used.

Seismicity Located in the Epicentral Region of the 3 May 1887 M_w 7.5 Earthquake

Here we evaluate in more detail the earthquakes located along the Basin and Range Province faults on the western margin of the Sierra Madre Occidental, including the seismicity along the faults that ruptured in 1887. Figure 7 shows the epicenters relocated in the epicentral region of the 3 May 1887 M_w 7.5 earthquake with the SSST method and velocity model V4 of Figure 3.

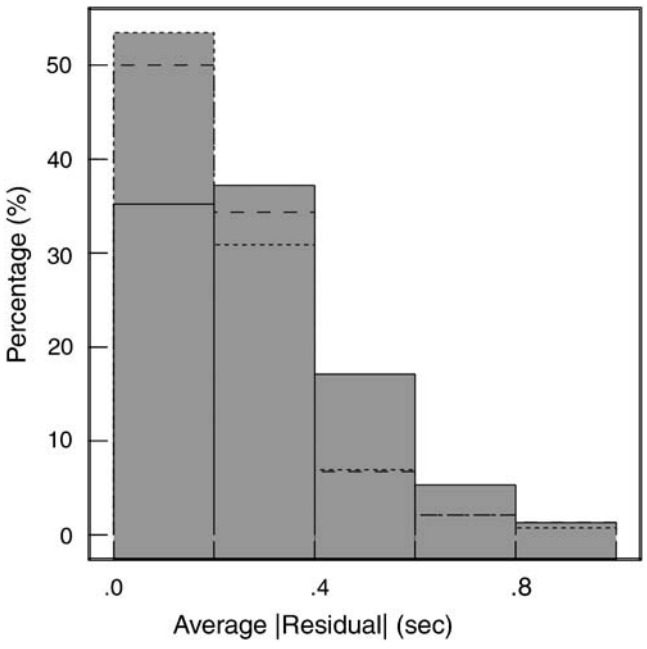

Figure 6. Histogram of the average absolute value of the travel-time residuals. Solid lines, Hypoinverse solutions, dashed lines, SSST relocations with velocity model V2 (see Fig. 2); dotted lines, relocations with velocity model V4.

As in the study by Natali and Sbar (1982), several events could be located west of the trace of the Pitáycachi fault. However, the seismicity recorded in this study during 2003–2007 does not extend as far north as documented by Natali and Sbar (1982) for events in 1978–1979. Apparently, there is currently no seismic activity in the northernmost part of the 1887 rupture. Farther south, many events are located west of the traces of the Teras and Otates faults (Fig. 7); they very likely originated on the Teras and Otates segments of the 1887 rupture. The microseismicity cluster west of station HUA suggests that an additional rupture segment may exist south of the Otates segment.

Our study shows that the west-dipping Villa Hidalgo and Granados normal-fault segments directly south of the 1887 surface rupture also are currently seismically active (Fig. 7). The locations of these events are well constrained because several stations are located in close vicinity on either flank of these two faults (Fig. 7). The Villa Hidalgo fault bounds the Angostura basin (Suter, 2008a), which is filled with evaporates and the syntectonic continental deposits of the Báucarit Formation. Field checking the fault trace east of Villa Hidalgo did not reveal any obvious morphological or stratigraphic evidence of Quaternary fault activity. The fault dips there between 58° and 78° W, and its throw is a minimum of 1,420 m. The trace of the Granados fault passes directly east of the towns of Granados and Huásabas (Montigny *et al.*, 1987, fig. 3), which were badly damaged in the 17 May 1913 (I_{max} VIII, M_I 5.0 ± 0.4) and 18 December 1923 (I_{max} IX, M_I 5.7 ± 0.4) earthquakes (Suter, 2001). These earthquakes may have been triggered by a slight Coulomb failure stress increase of <0.2 bar caused by the 1887 rupture (Suter and Contreras, 2002). We consider it likely that the 1913 and 1923 earthquakes resulted from partial ruptures of the Granados fault and that the recorded microearthquakes are aftershocks of these two events.

Microseismicity also seems to be associated with a symmetrical graben in the east–central part of Figure 7, the fault west of station MOC in the southwestern most part of Figure 7, and other fault segments in the west–central part of Figure 7, northwest of station NAC. It is therefore likely that these faults ruptured in the geologically recent past. Alternatively, this microseismicity may have been triggered by the 1887 rupture and related changes in the distribution of tectonic stress.

A major seismicity cluster near station NAC (Fig. 4) corresponds mostly to explosions at the La Caridad copper mine. We filtered out events near NAC occurring within the time range scheduled for mine blasts and with depths of less than 3 km. It cannot be excluded that some of the remaining events (Fig. 7) are of tectonic origin; some nearby epicenters are located west of the Basin and Range Province fault trace that passes west of station NAC.

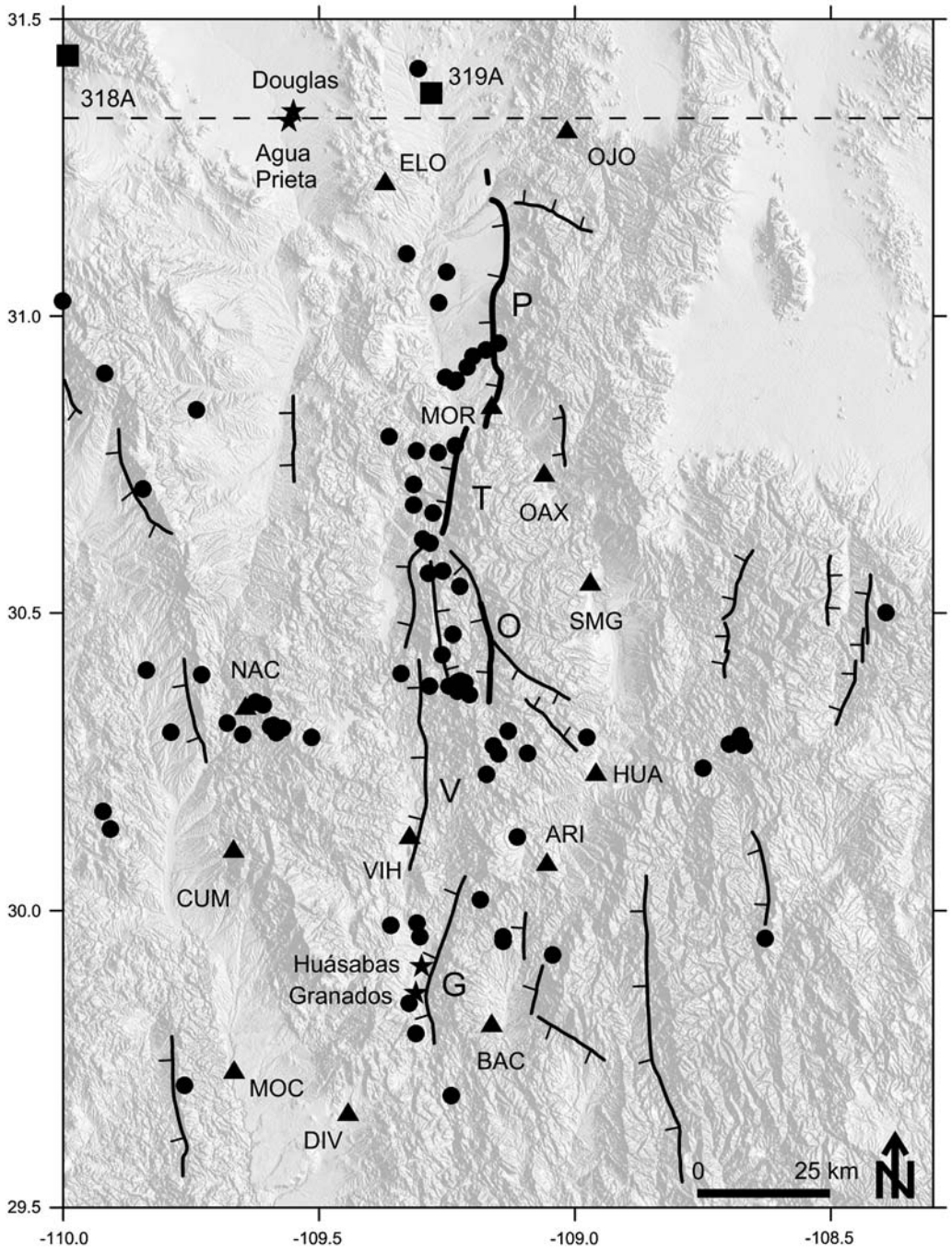

Figure 7. Distribution of epicenters near the 1887 rupture, relocated with the SSST method and velocity model V4. (The location of this figure closely corresponds to the three rectangles on the upper right side of Fig. 4). Most of the microseismicity clusters are on the faults that ruptured in 1887 (P, Pitáycachi; T, Teras; O, Otates) and the Villa Hidalgo (V) and Granados (G) faults. Further explanations are in the text.

Discussion

As previously described, the 3 May 1887 M_w 7.5 mainshock has been followed by a long-lasting series of aftershocks. The distribution of the aftershocks correlates well with calculated changes in Coulomb failure stress resulting from the 1887 earthquake (Suter and Contreras, 2002). Two major historical earthquakes in 1913 and 1923, as well as the microseismicity recorded in this study, indicate that the area of aftershock activity has increased southward along the same fault system. This may also be related to the southward direction of the 1887 rupture propagation and the related directivity effect.

Long-lasting (> 50 yr) series of aftershocks have also been documented for other large historical Basin and Range Province earthquakes (see references in Stein and Liu, 2009). Aftershocks following large midcontinental earthquakes, such as the 1811–1812 New Madrid and 1886 Charleston,

South Carolina, earthquakes, are known to persist for centuries (Mueller *et al.*, 2004; Li *et al.*, 2005). Geodynamic models by Li *et al.* (2007) show that large intraplate earthquakes can significantly increase Coulomb stress and strain energy in the surrounding crust. The strain energy release from a large earthquake will migrate to the surrounding region and may dominate the local strain energy budget for thousands of years following the mainshock, in contrast to interplate seismic zones, where strain energy is dominated by tectonic loading (Stein and Liu, 2009).

In a model of aftershock activity, Ebel *et al* (2000) combine the Omori Law of nearly hyperbolic temporal aftershock decay with the Gutenberg–Richter distribution of the rate of events as a function of magnitude. According to their model, the larger the magnitude of the mainshock, the greater is the current aftershock activity rate. As mentioned previously, the 1887 Sonora earthquake has the world's longest recorded normal-fault surface rupture in historic time and is the largest historical earthquake of the southern Basin and Range Province. An explanation of the long-lasting series of aftershocks of the 1887 Sonora earthquake, as compared to other Basin and Range Province earthquakes, could therefore be the large size of the mainshock.

A mechanical model of the rate of earthquake production by Dieterich (1994) predicts that aftershock duration is proportional to mainshock recurrence time. His compilation of these two parameters for historical earthquakes, which does not include Basin and Range Province earthquakes, appears consistent with the model prediction but has large scatter. As mentioned previously, the recurrence time of 1887-sized events on the Pitáycachi fault is 100–200 k.y. (Bull and Pearthree, 1988), which is near the upper end of the range of recurrence intervals of major normal faults in the southern Basin and Range Province and the Rio Grande rift (Machette, 1998). The duration of aftershock activity so far is a mere 0.1% of the recurrence time of the Pitáycachi fault. According to the model by Dieterich (1994), the long recurrence time of the Pitáycachi fault also indicates the observed microseismicity to be aftershock activity of the 1887 event.

Stein and Liu (2009) have analyzed the duration of aftershock sequences in various tectonic environments and hypothesize that many concentrations of midcontinental earthquakes are aftershocks of large events that occurred hundreds of years ago. According to their observations, the slower the fault slip rate, the longer is the aftershock duration. As mentioned previously, the Quaternary slip rate of the Pitáycachi fault is 0.015 mm/yr (Bull and Pearthree, 1988). No Quaternary slip rates have been documented for the Teras and Otates faults, but their geologic slip rates are 0.08 mm/yr and 0.06 mm/yr, respectively (Suter, 2008a and 2008b). Based on the compilations by McCalpin (1995) and dePolo and Anderson (2000), the slip rates of normal faults in the Great Basin and the southern Basin and Range Province range over four orders of magnitude. The slip rate of the Pitáycachi fault is at the very lower end of that range, which also supports the hypothesis that the observed microseismicity is aftershock activity of the 1887 event.

No seismicity was recorded to the southwest of the RESNES array; especially the Hermosillo region seems to be seismically quiescent (Fig. 4). The maximum secular strain rate in northeastern Sonora, as determined from very-long-baseline–interferometry (VLBI) space geodetic data extrapolated across the international boundary, is 0.8 to 1.2× 10^{-8} yr^{-1} with a two sigma error of 10% (Ward, 1998), whereas closer to the Gulf of California, the strain rate increases to 1.2 to 2 × 10^{-8} yr^{-1}. The lack of seismicity in the Hermosillo region, despite its higher strain rate, further supports the hypothesis that the recorded microseismicity results from the 1887 rupture.

Conclusions

We relocate the microseismicity in the epicentral region of the 3 May 1887 M_w 7.5 Sonora, Mexico, earthquake. This preinstrumental earthquake resulted from a cascading rupture of three normal faults, with an endpoint-to-endpoint surface rupture length of 101.8 km. It is characterized by a long-lasting aftershock series that continues to the present time.

The initial data set consisted of local and regional body-wave arrival times from nearly 600 local and regional events recorded during 2003–2007. We were able to relocate 80% of these events with a modified version of the COMPLOC code that permits the use of regional phases (*Pn*, *Pg*, *Sn*, *Sg*) and weights the phase arrival picks according to the source-station distance.

The relocated epicenters tend to align in more planar features than their original locations. Most of the events cluster in the upper crust near the faults that ruptured during the 1887 earthquake. However, the microseismicity does not extend as far north as documented by Natali and Sbar (1982) for events in 1978–1979; apparently, there is currently no seismic activity in the northernmost part of the 1887 rupture. Many of the events are located west of the traces of the Teras and Otates faults (Fig. 7); they very likely originated on the Teras and Otates segments of the 1887 rupture.

The area of microseismicity has increased southward with time along the same fault system. Our study shows that the west-dipping Villa Hidalgo and Granados normal faults, located south of the 1887 surface rupture, also are currently seismically active (Fig. 7). We consider it likely that the 1913 and 1923 earthquakes resulted from partial ruptures of the Granados fault and that the recorded microearthquakes are aftershocks of these two events.

The long aftershock duration of the 1887 mainshock is common for regions with a low deformation rate, such as the Basin and Range Province, and even more typical for intraplate regions, such as the midcontinental locations of the 1811–812 New Madrid and 1886 Charleston, South Carolina, earthquakes. Several models of aftershock activity predict aftershock activity rate to be proportional to the

magnitude of the mainshock (Ebel *et al.*, 2000), aftershock duration to be proportional to mainshock recurrence time (Dieterich, 1994), and aftershock duration to be indirectly proportional to fault slip rate (Stein and Liu, 2009). The 1887 Sonora earthquake qualitatively confirms all three models. The long aftershock duration can be explained by the unusually large magnitude of the mainshock and by the low slip rates and long mainshock recurrence times of the faults that ruptured in 1887. The strain energy release from the 1887 mainshock has migrated southward and is likely to dominate the local strain energy budget due to low tectonic far-field loading.

Data and Resources

An extensive 1887 earthquake bibliography (pdf files) is posted at www.geo.arizona.edu/gsat/1887eq/bibliography.html. It includes the digitized 1888 report by José Guadalupe Aguilera. The seismograms used in this article were recorded by stations of the Red Sísmica del Noreste de Sonora (RESNES) seismic array and the USArray. Data from the RESNES network can be requested from the first author of this article. USArray data are available through the Incorporated Research Institutions for Seismology Data Management Center (http://www.iris.edu/USArray). Some plots were made using the Generic Mapping Tools (www.soest.hawaii.edu/gmt; Wessel and Smith, 2009). The digital elevation models in Figures 4 and 7 were created from Shuttle Radar Topography Mission data with Surfer® Version 9 (www.goldensoftware.com).

Acknowledgments

The installation and operation of the Red Sísmica del Noreste de Sonora (RESNES; Seismic Network of Northeastern Sonora) has been possible thanks to the financial support of the Consejo Nacional de Ciencia y Tecnología (CONACYT; Mexican National Council for Science and Technology) by means of the projects G33102-T and 59216. Carlos Huerta has provided logistic support since 2008. We are also grateful for the technical assistance given by Luis Inzunza, Antonio Mendoza, Arturo Pérez Vertti, and Ignacio Méndez. We are thankful for the participation of Alejandro Hurtado from the Instituto de Geología de la Universidad Nacional Autónoma de México and the participation of Oscar Romero during the initial part of the project. This article was written while one of us (R. R. C) was a UC MEXUS-CONACYT Visiting Scholar at the University of California, San Diego, Institute of Geophysics and Planetary Physics, Scripps Institution of Oceanography. We thank Seth Stein for making his preprint about long-duration aftershock sequences accessible to us. The comments and suggestions by two anonymous reviewers are appreciated.

References

Aguilera, J. G. (1888). Estudio de los fenómenos séismicos del 3 de mayo de 1887, *Anales del Ministerio de Fomento de la República Mexicana* **10,** 5–56.

Astiz, L., P. M. Shearer, and C. Agnew (2000). Precise relocations and stress change calculations for the Upland earthquake sequence in southern California, *J. Geophys. Res.* **105,** 2937–2853.

Bull, W. B., and P. A. Pearthree (1988). Frequency and size of Quaternary surface rupture of the Pitáycachi fault, northeastern Sonora, Mexico, *Bull. Seismol. Soc. Am.* **78,** 956–978.

Castro, R. R., C. Condori, O. Romero, C. Jacques, and M. Suter (2008). Seismic attenuation in northeastern Sonora, Mexico, *Bull. Seismol. Soc. Am.* **98,** 722–732.

Castro, R. R., O. M. Romero, and M. Suter (2002). Red sísmica para el monitoreo de la sismicidad del sistema de fallas normales del noreste de Sonora, *GEOS* **22,** 379 (in Spanish).

Clayton, R. W., J. Trampert, C. J. Rebollar, J. Ritsema, P. Persaud, H. Paulssen, X. Pérez-Campos, A. van Wettum, A. Pérez-Vertti, and F. diLuccio (2004). The NARS-Baja array in the Gulf of California rift zone, *Margins Newsl.* **13,** 1–4.

dePolo, C. M., and J. G. Anderson (2000). Estimating the slip rates of normal faults in the Great Basin, USA, *Basin Res.* **12,** 227–240.

dePolo, C. M., D. G. Clark, D. B. Slemmons, and A. R. Ramelli (1991). Historical surface faulting in the Basin-and-Range province, western North America—Implications for fault segmentation, *J. Struct. Geol.* **13,** 123–136.

Dieterich, J. H. (1994). A constitutive law for rate of earthquake production and its application to earthquake clustering, *J. Geophys. Res.* **99,** 2601–2618.

Ebel, J. E., K. P. Bonjer, and M. C. Oncescu (2000). Paleoseismicity: Seismicity evidence for past large earthquakes, *Seismol. Res. Lett.* **71,** 283–294.

Goodfellow, G. E. (1888). The Sonora earthquake, *Science* **11,** 162–166.

Harder, S., and G. R. Keller (2000). Crustal structure determined from a new wide-angle seismic profile in southwestern New Mexico, in *Southwest Passage: A Trip through the Phanerozoic, New Mexico Geological Society Guidebook*, Fall Field Conference Guidebook-51, T. W. Lawton, N. J. McMillan, and V. T. McLemore (Editors), New Mexico Geological Society, Socorro, New Mexico, 75–78.

Jackson, J. A. (2002). Using earthquakes for continental tectonic geology, in *International Handbook of Earthquake and Engineering Seismology, Part A*, W. H. K. Lee, H. Kanamori, P. C. Jennings, and C. Kisslinger (Editors), San Diego, California, Academic Press, part A, 491–503.

Klein, F. W. (2002). User's guide to HYPOINVERSE-2000, a Fortran program to solve for earthquake locations and magnitudes, *U.S. Geol. Surv. Open-File Rept. 02-171*, 121 pp.

Li, Q., M. Liu, and E. Sandvol (2005). Stress evolution following the 1811–1812 large earthquakes in the New Madrid seismic zone, *Geophys. Res. Lett.* **32,** L11310, doi 10.1029/2004GL022133.

Li, Q., M. Liu, Q. Zhang, and E. Sandvol (2007). Stress evolution and seismicity in the central–eastern United States: Insights from geodynamic modeling, Geological Society of America Special Paper 425, in *Continental Intraplate Earthquakes: Science, Hazard, and Policy Issues*, S. Stein and S. Mazzotti (Editors), 149–166.

Lin, G., and P. M. Shearer (2005). Tests of relative earthquake location techniques using synthetic data, *J. Geophys. Res.* **110,** no. B04304, doi 10.1029/2004JB003380.

Lin, G., P. M. Shearer, E. Hauksson, and C. H. Thurber (2007). A three-dimensional crustal seismic velocity model for southern California from a composite event method, *J. Geophys. Res.* **112,** doi 10.1029/2007JB004977.

Machette, M. N. (1998). Contrasts between short-term and long-term records of seismicity, in *The Río Grande Rift—Important Implications for Seismic-Hazard Assessments in Areas of Slow Extension, Basin and Range Province Seismic-Hazards Summit*, Miscellaneous Publication 98-2, W. R. Lund (Editor), Utah Geological Survey, Salt Lake City, Utah, 84–95.

McCalpin, J. P. (1995). Frequency distribution of geologically determined slip rates for normal faults in the western United States, *Bull. Seismol. Soc. Am.* **85,** 1867–1872.

Menges, C. M., and P. A. Pearthree (1989). Late Cenozoic tectonism in Arizona and its impact on regional landscape evolution, *Arizona Geological Society Digest* **17,** 649–680.

Montigny, R., A. Demant, P. Delpretti, P. Piguet, and J. J. Cochemé (1987). Chronologie K/Ar des séquences volcaniques tertiaires du nord de la Sierra Madre Occidental (Mexique), *Comptes Rendus de l'Académie des Sciences*, série II, **304,** no. 16, 987–992.

Mueller, K., S. E. Hough, and R. Bilham (2004). Analysing the 1811–1812 New Madrid earthquakes with recent instrumentally recorded aftershocks, *Nature* **429,** 284–288.

Natali, S. G., and M. L. Sbar (1982). Seismicity in the epicentral region of the 1887 northeastern Sonora earthquake, Mexico, *Bull. Seismol. Soc. Am.* **72,** 181–196.

Orozco y Berra, J. (1887). Efemérides séismicas Mexicanas, *Memorias de la Sociedad Científica Antonio Alzate* **1,** 303–541.

Orozco y Berra, J. (1888). Efemérides séismicas Mexicanas, adiciones y rectificaciones, *Memorias de la Sociedad Científica Antonio Alzate* **2,** 261–288.

Parsons, T. (1995). The Basin and Range Province, in *Continental Rifts: Evolution, Structure, Tectonics*, K. H. Olsen (Editor), Elsevier, Amsterdam, 277–324.

Pearthree, P. A., and S. S. Calvo (1987). The Santa Rita fault zone: evidence for large magnitude earthquakes with very large recurrence intervals, Basin and Range Province of southeastern Arizona, *Bull. Seismol. Soc. Am.* **77,** 97–116.

Richards-Dinger, K., and P. Shearer (2000). Earthquake locations in southern California obtained using source-specific station terms, *J. Geophys. Res.* **105,** 10,939–10,960.

Sbar, M. L., and S. M. DuBois (1984). Attenuation of intensity for the 1887 northern Sonora, Mexico earthquake, *Bull. Seismol. Soc. Am.* **74,** 2613–2628.

Shearer, P. M. (1997). Improving local earthquake locations using the L1 norm and waveform cross correlation: Application to the Whittier Narrows, California, aftershock sequence, *J. Geophys. Res.* **102,** 8269–8283.

Stein, S., and M. Liu (2009). Long aftershock sequences within continents and implications for earthquake hazard assessment, *Nature* **462,** 87–89.

Suter, M. (2001). The historical seismicity of northeastern Sonora and northwestern Chihuahua, Mexico (28–32° N, 106–111° W), *J. S. Am. Earth Sci.* **14,** 521–532.

Suter, M. (2006). Contemporary studies of the 3 May 1887 M_w 7.5 Sonora, Mexico (Basin and Range Province) earthquake, *Seismol. Res. Lett.* **77,** no. 2, 134–147.

Suter, M. (2008a). Structural configuration of the Otates fault (southern Basin and Range Province) and its rupture in the 3 May 1887 M_w 7.5 Sonora, Mexico, earthquake, *Bull. Seismol. Soc. Am.* **98,** 2879–2893.

Suter, M. (2008b). Structural configuration of the Teras fault (southern Basin and Range Province) and its rupture in the 3 May 1887 M_w 7.5 Sonora, Mexico earthquake, *Revista Mexicana de Ciencias Geológicas* **25,** 179–195.

Suter, M., and J. Contreras (2002). Active tectonics of northeastern Sonora, Mexico (southern Basin and Range Province) and the 3 May 1887 M_w 7.4 earthquake, *Bull. Seismol. Soc. Am.* **92,** 581–589.

Trampert, J., H. Paulsen, A. Van Wettum, J. Ritsema, R. Clayton, R. Castro, C. Rebollar, and A. Pérez-Vertti (2003). New array monitors seismic activity near the Gulf of California in México, *EOS, Trans. AGU* **84,** 29–32.

Vázquez, L. (1887). El terremoto del 3 de Mayo, *La Constitución, Periódico Oficial del Gobierno del Estado* (Hermosillo, Sonora) **9,** no. 24, 1–2.

Wallace, T. C., and P. A. Pearthree (1989). Recent earthquakes in northern Sonora, *Arizona Geology* **19,** no. 3, 6–7.

Wallace, T. C., A. M. Domitrovic, and P. A. Pearthree (1988). Southern Arizona earthquake update, *Arizona Geology* **18,** no. 4, 6–7.

Ward, S. N. (1998). On the consistency of earthquake moment rates, geological fault data, and space geodetic strain: The United States, *Geophys. J. Int.* **134,** 172–186.

Wells, D. L., and K. J. Coppersmith (1994). New empirical relationships among magnitude, rupture length, rupture width, rupture area, and surface displacement, *Bull. Seismol. Soc. Am.* **84,** 974–1002.

Wessel, P., and W. H. F. Smith (2009). The Generic Mapping Tools (GMT) version 4.5.0 technical reference & cookbook, SOEST/NOAA, available at http://gmt.soest.hawaii.edu.

Yeats, R. S., K. Sieh, and C. R. Allen (1997). *The Geology of Earthquakes*, Oxford University Press, Oxford, United Kingdom, 568 p.

Centro de Investigación Científica y de Educación Superior de Ensenada (CICESE)
División Ciencias de la Tierra
Departamento de Sismología
km 107 Carretera Tijuana-Ensenada
22860 Ensenada, Baja California, México
raul@cicese.mx
(R.R.C.)

Institute of Geophysics and Planetary Physics
Scripps Institution of Oceanography
University of California, San Diego
La Jolla, California 92093
pshearer@ucsd.edu
pshearer@ucsd.edu
(P.M.S., L.A., F.V.)

Instituto de Geología
Universidad Nacional Autónoma de México (UNAM)
Estación Regional del Noroeste
Apartado Postal 1039
83000 Hermosillo, Sonora, México
Max.Suter@ensi.ch
jacques@geologia.unam.mx
(M.S., C.J.)

Manuscript received 15 July 2009